UNIVERSITY OF BIRMINGHAM

University of Birmingham
Research at Birmingham

A real-time analysis of GFP unfolding by the AAA+ unfoldase PAN

Krüger, Georg; Kirkpatrick, John P.; Mahieu, Emilie; Franzetti, Bruno; Gabel, Frank; Carlomagno, Teresa

[Link to publication on Research at Birmingham portal](#)

A real-time analysis of GFP unfolding by the AAA+ unfoldase PAN

Georg Krüger [a], John Kirkpatrick [b], Emilie Mahieu [c], Bruno Franzetti [c], Frank Gabel [c], Teresa Carlomagno [b,*]

[a] *Institute of Organic Chemistry and Centre of Biomolecular Drug Design, Leibniz University Hannover, Schneiderberg 38, D-30167 Hannover, Germany*
[b] *School of Biosciences, College of Life and Environmental Sciences, University of Birmingham, Edgbaston, B15 2TT Birmingham, United Kingdom*
[c] *Univ. Grenoble Alpes, CEA, CNRS, IBS, 71 avenue des Martyrs, F-38000 Grenoble, France*

ARTICLE INFO

ABSTRACT

Protein quality control systems are essential to maintain a healthy proteome. They often consist of an unfoldase unit, typically an AAA+ ATPase, coupled with a protease unit. In all kingdoms of life, they function to eliminate misfolded proteins, and thus prevent that their aggregates do harm to the cell, and to rapidly regulate protein levels in the presence of environmental changes. Despite the huge progress made in the past two decades in understanding the mechanism of function of protein degradation systems, the fate of the substrate during the unfolding and proteolytic processes remains poorly understood. Here we exploit an NMR-based approach to monitor GFP processing by the archaeal PAN unfoldase and the PAN–20S degradation system in real time. We find that PAN-dependent unfolding of GFP does not involve the release of partially-folded GFP molecules resulting from futile unfolding attempts. In contrast, once stably engaged with PAN, GFP molecules are efficiently transferred to the proteolytic chamber of the 20S subunit, despite the only weak affinity of PAN for the 20S subunit in the absence of substrate. This is essential to guarantee that unfolded but not proteolyzed proteins are not released into solution, where they would form toxic aggregates. The results of our studies are in good agreement with previous results derived from real-time small-angle-neutron-scattering experiments and have the advantage of allowing the investigation of substrates and products at amino-acid resolution.

1. Introduction

For a "healthy-life", cells need to strictly monitor the folding status and the activity of their protein components, which can either unfold/misfold during synthesis or be denatured by stress events, such as heat, oxidation and environmental changes. Inactive or unfolded proteins interfere with cellular functions and need to be cleared by either refolding or degradation. Both chaperones and proteases are part of the protein quality control system, with the first class of enzymes assisting protein folding and the second degrading misfolded protein chains. AAA+ (ATPases associated with diverse cellular activities) unfoldases constitute a class of proteins that associate with either chaperones or proteases to either refold or degrade misfolded proteins and prevent the accumulation of toxic aggregates [1–3]. AAA+ unfoldases exist in all three kingdoms of life. In eukaryotes and archaea, the proteolytic complex formed by an AAA+ unfoldase and a protease is called the proteasome [4], while in bacteria unfoldases and proteases of the Clp family associate to form similar proteolytic machineries [5]. In addition to their

function as a cellular "garbage disposal system", the proteolytic complexes have a pivotal role in the regulation of protein activity. In living and proliferating cells, protein activity-levels are controlled both spatially and temporally. Next to regulation of gene expression, one way of adjusting protein levels rapidly in response to changing environmental conditions consists of the degradation of superfluous protein copies by the proteolytic enzymes [6].

The proteolytic machinery consists of a compartmentalized complex comprising an hexameric AAA+ unfoldase and an heptameric protease. The 26S eukaryotic proteasome, for example, comprises a 19S AAA+ ATPase regulatory particle (RP) and a 20S proteolytic core particle (CP) [5]. Accessory proteins are associated with the RP in eukaryotes but not in archaea. The last two decades have seen enormous progress in our understanding of the functional mechanism of proteasomal complexes. Several cryo-electron-microscopy (EM) structures of proteolytic machinery [3,7–14] with and without substrate have converged on a possible mechanism for unfolding and translocation to the protease chamber: in this "hand-over-hand" mechanism, the substrate is passed from one unfoldase subunit to the other, while the unfoldase hexameric ring uses energy from ATP hydrolysis to cycle clockwise through a spiral staircase arrangement (sequential model). The

structures have also revealed a correlation between the nucleotide bound state of the AAA+ unfoldase subunit and its engagement with the substrate. Single-molecule experiments of the bacterial proteolytic machinery ClpXP have linked the number of hydrolysed ATP molecules with the length of the translocated peptide sequence and have challenged the sequential model by demonstrating that translocation occurs in bursts (stochastic model) rather than sequentially [15–18]. Despite so many insights into the functional mechanism of the proteolytic machinery, detailed quantitative information on the fate of the substrate during the process remains scarce. An NMR study of the unfolding of calmodulin by the VAT AAA+ unfoldase from *Thermoplasma acidophilum*, which used covalent tethering of the substrate to the enzyme at multiple stages during the unfolding reaction, demonstrated that the N-terminal lobe of calmodulin unfolds cooperatively when pulled from the N-terminus, while the C-terminal lobe unfolds stepwise [19]. In another study [20,21], small-angle neutron scattering (SANS) in combination with contrast-matching was used to study the unfolding and degradation of GFP (green fluorescent protein) by the archaeal PAN AAA+ ATPase in complex with the 20S archaeal CP. The authors found that the GFP degradation process is biexponential and that the rates of degradation correlate strongly with ATP hydrolysis [20]. Furthermore, in these ensemble studies the average fraction of partially unfolded GFP tethered to the proteolytic machinery was found to be always less than 0.05–0.1, even if the enzyme:substrate stoichiometric ratio at the beginning of the reaction was ∼0.3. This is compatible with the notion that not all encounter events between substrate and enzyme result in active translocation.

Here, we use methyl-TROSY nuclear magnetic resonance (NMR) spectroscopy to monitor the unfolding process of GFP in solution in the presence of either PAN or the PAN–20S proteasome complex from the thermophilic archaeon *Methanocaldococcus jannaschii* (*Mj*) under turn-over conditions. Our goal is to measure residue-dependent unfolding and degradation time constants to determine whether GFP processing involves the formation and release of partially unfolded intermediates. Furthermore, we aim to obtain detailed structural information on the products of the unfolding reaction. Using an enzyme from a thermophilic archaeon gives us the ability to slow down the reaction at intermediate temperatures, which, in combination with SOFAST-HMQC experiments [22] allows the reaction to be followed over several turn-over cycles. We find that the unfoldase machinery is tightly coupled to the proteasome and no long-lived unfolded intermediate is released into solution during the substrate processing reaction.

2. Material and Methods

2.1. Cloning

A restriction-free cloning approach was used to generate all expression constructs [23]. Cloning results were verified by DNA sequencing.

The green fluorescent protein (GFP) used in this study is a folding-reporter GFP variant [24]. We obtained a synthetic gene (GeneCust Europe) coding for monomeric GFPuv mutant A206K [25] with a C-terminal ssrA tag (AANDENYALAA), necessary for targeting to PAN. The gene was cloned into the pETM11 expression vector (EMBL collection) with an N-terminal His$_6$ tag followed by a TEV (tobacco etch virus) protease cleavage-site. Two additional mutations F64L and S65T were introduced to achieve a GFP variant with improved expression yields and enhanced stability. The mutations were introduced using the QuikChange kit (Agilent Technology).

The codon-optimized gene of *Methanocaldoccus jannaschii* PAN was obtained from GeneCust Europe and was cloned into the

pET30a expression-vector carrying a C-terminal His$_6$ tag. This construct of PAN (PAN-His$_6$) is not compatible with binding to the 20S CP, which requires an accessible C-terminal HbYX-motif. Thus, to reconstitute the proteolytic complex, we cloned the PAN gene into the pETM22 expression-vector (EMBL collection), coding for an N-terminal thioredoxin solubility tag (Trx), a His$_6$ purification tag and a 3C-protease cleavage site (Trx-PAN).

The *Methanocaldoccus jannaschii* 20S CP consists of α- and β-subunits. Their codon-optimized synthetic genes were obtained from GeneCust Europe and cloned into pET28a and pET30a expression vectors, respectively. The α-subunit carried an N-terminal His$_6$-tag, while the β-subunit, including the 6-residue N-terminal pro-peptide, was untagged.

2.2. Protein expression

All proteins were expressed in *E. coli* BL21 (DE3) cells grown in media containing 50 µg/ml kanamycin (Carl Roth). For GFP-ssrA, freshly transformed *E. coli* BL21 (DE3) cells were grown overnight in lysogeny broth (LB) at 37 °C. The next day, the overnight culture was diluted 1:100 in LB medium and cells were grown at 37 °C to an OD$_{600}$ of 0.8. Cells were then cooled to 20 °C and expression of GFP-ssrA was induced by addition of 0.1 mM isopropyl-β-D-thiogalactoside (IPTG, Carl Roth). The cell culture was kept at 20 °C for 8 h, after which cells were harvested by centrifugation (5000 g at 4 °C for 20 min), washed with ice-cold phosphate-buffered saline (PBS) and stored at –80 °C until further use. Production of isotopically enriched GFP-ssrA was carried out in M9 minimal medium. Uniformly ^{13}C, ^{15}N-labelled proteins (GFP-ssrA) were expressed in M9 minimal medium containing 1 g/l ^{15}NH$_4$Cl and 4 g/l ^{13}C$_6$-D-glucose (Eurisotop and Sigma Aldrich). For protein purification, cells were resuspended in lysis buffer (50 mM Tris-HCl pH 7.5, 100 mM NaCl, 10 mM imidazole, 5 mM β-mercaptoethanol) supplemented with DNAse I (Roche), complete EDTA-free protease inhibitors (Roche), lysozyme (Carl Roth) and 20 mM MgSO$_4$ and incubated for 20 min. After sonication, the cell debris was removed by centrifugation (19000 g, 4 °C, 1 h) and the cleared lysate was loaded onto a 5 ml HisTrap HP IMAC column (Cytiva). The column was washed with 20 column volumes (CV) of lysis buffer to remove unbound species and the His$_6$-protein was eluted with 500 mM imidazole in lysis buffer. The N-terminal His$_6$-tag was cleaved overnight with TEV-protease during dialysis against lysis buffer to remove the imidazole. The solution was then applied to the HisTrap HP IMAC column to separate the tag, uncleaved His$_6$-protein and the His$_6$-tagged TEV-protease from the cleaved GFP-ssrA, which was contained in the flow-through. The solution containing GFP-ssrA was concentrated with a 10-kDa MWCO Amicon centrifugal filter unit (Millipore) and further purified by size-exclusion chromatography using a HiLoad 16/600 Superdex S75 pg column (Cytiva) in storage buffer (20 mM Tris-HCl pH 7.5, 100 mM NaCl). The purified protein was concentrated, aliquoted and stored at –80 °C until further use. The integrity of GFP-ssrA after purification was confirmed by ESI mass spectrometry.

For PAN, freshly transformed *E. coli* BL21 (DE3) cells were grown overnight in LB at 37 °C. The next day, the overnight culture was diluted 1:100 in LB medium and cells were grown at 37 °C to an OD$_{600}$ of 0.75. Cells were then cooled to 20 °C and expression of PAN was induced by the addition of IPTG (1 mM for PAN-His$_6$, 0.1 mM for Trx-PAN). Cells were incubated at 20 °C for a further 18 h, harvested by centrifugation (5000 g at 4 °C, 20 min), washed with PBS and stored at –80 °C until further use. Cells producing Trx-PAN were resuspended in lysis-buffer A (20 mM Tris-HCl pH 7.5, 500 mM NaCl, 10 mM MgCl$_2$, 10 mM imidazole and 5 mM β-mercaptoethanol) supplemented with DNAse I (Roche), RNAse (Roche), complete EDTA-free protease inhibitor cocktail (Roche)

and lysozyme. After enzymatic lysis for 20 min followed by sonication, the cell debris was removed by centrifugation (19000 g, 4 °C, 1 h) and the cleared lysate was loaded onto a 5 ml HisTrap HP IMAC column (Cytiva). The column was washed with 20 column volumes (CV) of lysis buffer A to remove unbound species and Trx-PAN was eluted with a gradient of 50–500 mM imidazole in 10 CVs. Peak-fractions were exchanged into lysis buffer A using a HiPrep 26/10 desalting column and the Trx-His$_6$-tag was cleaved overnight with 3C protease. The solution was then applied to the HisTrap HP IMAC column to separate the His$_6$-Trx tag, non-cleaved Trx-PAN and His$_6$-tagged 3C protease from the cleaved PAN, which was contained in the flow-through. Cleaved PAN was buffer-exchanged to the storage buffer A (20 mM Tris-HCl pH 7.5, 100 mM NaCl, 10 mM MgCl$_2$) and further purified by anion exchange chromatography on a 5 ml HiTrap Q HP column. Finally, PAN was purified on a HiLoad 16/600 Superdex 200 pg size exclusion chromatography (SEC) column in storage buffer A, concentrated using a 100-kDa MWCO Amicon centrifugal filter (Millipore) and stored at –80 °C.

Cells producing PAN-His$_6$ were lysed in storage buffer A supplemented with 5 mM imidazole, DNAse I (Roche), RNAse (Roche), lysozyme, complete EDTA-free protease inhibitor cocktail (Roche), 1 mg/ml AEBSF protease inhibitor and 0.1 % (v/v) Triton X-100 (Sigma Aldrich), lysed and centrifuged as for the Trx-PAN construct and the cleared lysate was loaded onto a 5 ml HisTrap HP IMAC column (Cytiva). The column was washed with 10 CVs of storage buffer A containing 25 mM imidazole and 10 CVs of the same buffer containing 50 mM imidazole. PAN-His$_6$ was eluted with 500 mM imidazole. PAN-His$_6$ was buffer-exchanged into storage buffer A and the purification proceeded as for cleaved PAN from the Trx-PAN construct.

Individual subunits of the *Methanocaldoccus jannaschii* 20S CP were expressed separately. Freshly transformed *E. coli* BL21 (DE3) cells harbouring either the pET28a-20S-α-subunit or the pET30a-20S-β-subunit plasmids were grown overnight in LB at 37 °C. The next day, the overnight culture was diluted 1:100 in LB medium and cells were grown at 37 °C to an OD$_{600}$ of 0.8. Cells were then cooled to room temperature and expression of PAN was induced by the addition of 1 mM IPTG. Cells were incubated at 20 °C for a further 18 h, harvested by centrifugation (5000 g at 4 °C, 20 min), washed with PBS and stored at –80 °C until further use. Cells expressing the α-subunits were resuspended in lysis buffer B (20 mM Tris-HCl pH 7.5, 100 mM NaCl, 10 mM MgCl$_2$, 5 mM imidazole), supplemented with complete EDTA-free protease inhibitor cocktail (Roche), DNAse I (Roche), lysozyme (Carl Roth, Germany), incubated at room temperature for 15 min and lysed by sonication. The cell debris was removed by centrifugation at 19,000 g and 4 °C for 1 h. The cleared lysate was loaded onto a HisTrap HP 5 ml column (Cytiva) pre-equilibrated in lysis buffer B. The column was washed with 10 column volumes (CV) of lysis buffer B to remove unbound species and 20S-α-subunits were eluted with 500 mM imidazole in lysis buffer B and then buffer-exchanged into storage buffer A (20 mM Tris-HCl pH 7.5, 100 mM NaCl, 10 mM MgCl$_2$) with a HiPrep 26/10 desalting column (Cytiva). The solution was then applied to a HiTrap Q HP 5 ml column (Cytiva) and the α-subunit was eluted with a gradient of 100–500 mM NaCl in 10 CVs. The fractions containing the α-subunit were concentrated (Amicon 15, 10-kDa MWCO, Millipore) and further purified by size-exclusion chromatography with a HiLoad 16/600 Superdex 200 pg column in storage buffer A. The fractions corresponding to single heptameric α-rings were collected and kept at 4 °C until further use.

Cells expressing the β-subunit were resuspended in storage buffer A, supplemented with protease inhibitors, DNAse and lysozyme, incubated at room temperature for 15 min and lysed with a high-pressure homogenizer (Avestin Emulsiflex C5, 15,000 psi).

The lysate was cleared by centrifugation (19000 g at 4 °C for 1 h) and loaded onto a 5 ml HiTrap SP HP cation exchange column (GE Healthcare) preequilibrated in storage buffer A. The column was washed with 10 CV of storage buffer A and the β-subunit was eluted with a 20 CV gradient of 100–1000 mM NaCl. The fractions containing the β-subunit were concentrated (Amicon-15, 10-kDa MWCO, Millipore) and further purified by size-exclusion chromatography with a HiLoad 16/600 Superdex 75 pg column in storage buffer A.

The 20S CP was assembled from the individual subunit following an established protocol [26]. Briefly, purified but not concentrated fractions from the size-exclusion purification containing β-subunit were mixed with α-rings and gently shaken at 37 °C for 6 h (volume ≈ 30 ml). 0.02 % NaN$_3$ (Sigma Aldrich) was added to prevent microbial growth. Next, the solution was concentrated to 2 ml (Amicon-15, 100-kDa MWCO, Millipore) at ambient temperature and further incubated at 37 °C for 16 h. Finally, the assembled 20S CP was purified by size-exclusion chromatography using a HiLoad 16/600 Superdex 200 pg column in storage buffer A. Fractions containing the $\alpha_7\beta_7\beta_7\alpha_7$ particle were collected, concentrated and stored at –80 °C until further use. Pro-peptide auto-catalysis of the β-subunits was confirmed by ESI-mass spectrometry.

2.3. NMR experiments

NMR spectra were recorded on Bruker Avance III HD 600-MHz (resonance assignment experiments) and 850-MHz (resonance assignments and time-course experiments) spectrometers running TopSpin 3.2 software and equipped with N$_2$-cooled and He-cooled inverse HCN triple-resonance cryogenic probes, respectively. Spectra were processed with TopSpin 3.2 (time-course experiments) or NMRPipe [27] (all other experiments) and analysed in CcpNmr Analysis v2.4 [28].

2.4. GFP resonance assignments

Backbone resonance assignments of folding-reporter GFP-ssrA were obtained from 2D ^{15}N-HSQC, 3D HNCO, 3D HN(CO)CACB and 3D HNCACB spectra measured at 42 °C on U-[^{15}N, ^{13}C] labelled protein at 600 μM concentration in storage buffer (20 mM Tris-HCl pH 7.5, 100 mM NaCl, 10 mM MgCl$_2$, 10 % D2O). A set of side-chain assignment experiments consisting of 2D constant-time ^{13}C-HSQC [29,30], 3D HCCH-TOCSY [31] and 3D H(CCCO)NH [32] spectra were recorded on the same sample for assignment of methyl groups. Met-ε assignments were obtained from a 3D ^{13}C-HMQC-NOESY-^{13}C-HMQC spectrum, comparing the experimental inter-methyl NOE peaks with those predicted from the GFP crystal structure (PDB entry 2B3Q). Assignments were transferred to 55 °C and 60 °C with the aid of a series of constant-time ^{13}C-HSQC spectra acquired at different temperatures.

2.5. Time-dependent NMR experiments to monitor unfolding and proteolysis

Time-dependent spectra were recorded during either the unfolding or the proteolytic reaction using 180 μl GFP-ssrA solution in standard 3-mm NMR tubes. Prior to the experiments, all buffer and protein solutions were carefully degassed to avoid formation of bubbles at the elevated temperature of the assays. All samples were in a 90%:10% H$_2$O:D$_2$O buffer containing 20 mM Tris-HCl pH 7.5, 100 mM NaCl, 100 mM ATP and 100 mM MgCl$_2$. RF pulses were calibrated on a sample of pure buffer. For the unfolding or proteolytic reactions, 100 μM of U-[^{15}N, ^{13}C] GFP-ssrA was mixed with either 5 μM unlabelled PAN or 5 μM PAN and 5 μM 20S, respectively. 100 mM ATP was added immediately before transfer to the NMR tube. The reaction was initiated by

transferring the tube to the spectrometer probe, which had been pre-heated to either 55 °C or 60 °C. A series of SOFAST-^{13}C-HMQC [33] spectra was started after the temperature inside the sample had stabilized (as judged from the ^{2}H lock signal). The total dead-time was 2.5–3 min. SOFAST-HMQC parameters optimized for the 100 μM ^{15}N,[13]C-GFP-ssrA sample included the 120° flip-angle for the excitation pulse, the recycle delay (150 ms) and the acquisition time in the directly detected dimension (50 ms). Each spectrum was recorded with 2 scans for a total of 100 s. After recording 18 2D SOFAST-HMQC spectra, we recorded a 1D ^{1}H proton spectrum to monitor the degree of ATP hydrolysis and verify the quality of the shimming. A full time-series consisted of six blocks of 18 spectra. Each condition was repeated three and two times at 60 and 55 °C, respectively.

2.6. Fluorescence measurements of GFP-ssrA unfolding and degradation

Unfolding and degradation of GFP-ssrA by PAN and PAN–20S, in buffer containing 20 mM Tris-HCl, pH 7.5, 100 mM NaCl, 100 mM MgCl$_2$ (Sigma Aldrich) and 100 mM ATP (Carl Roth), was monitored in a StepOne RT-PCR system (Thermo Scientific) through the loss of the intrinsic GFP fluorescence. 100 μM GFP-ssrA was incubated either with 5 μM PAN alone or with 5 μM PAN and 5 μM 20S in a final volume of 25 μl and fluorescence was measured at 60 °C in 10 s intervals. All runs were repeated in triplicate. ROX-dye filters were used to prevent detector saturation.

3. Theory and calculations

Pseudo-3D spectra from the time-series were analysed in CcpNmr Analysis. Peaks were automatically picked in all pseudo-3D planes. Peak intensities were obtained as peak-heights for which the spectral noise was taken as the experimental error. Intensity changes for all peaks from either three or two replicates (for the data at either 60 or 55 °C, respectively) were fitted to three different decay models using non-linear curve-fitting in OriginPro 9.1 (Origin Lab):

$$I = A \cdot e^{\left(\frac{-t}{T_{decay}}\right)} + I_0 \tag{1}$$

$$I(t) = A \cdot e^{\left(\frac{-t}{T_{decay}}\right)} + B \cdot t + I_0 \tag{2}$$

$$I(t) = A_1 \cdot e^{\left(\frac{-t}{T_{decay,1}}\right)} + A_2 \cdot e^{\left(\frac{-t}{T_{decay,2}}\right)} + I_0 \tag{3}$$

For each sampled peak, the triplicate measurements were used to assess statistical significance. The F-test was used to quantify the improvement of the fit with the increasing complexity of the fit-functions for each peak through all repetitions using the formula:

number of parameters (the alternative hypothesis, i.e. either ExpDec1 or ExpDec2); $DF_{null,1/2/3}$ and $DF_{alt,1/2/3}$ are the corresponding numbers of degrees-of-freedom (number of data-points less the number of fit-parameters). A (right-tailed) F probability distribution was calculated in Excel using the combined average F-ratio F_{avg} and the normalized number of degrees-of-freedom, i.e. the sum of degrees-of-freedom across all repetitions, divided by the number of repetitions. If the p-value was < 0.05, the model with the higher number of parameters was deemed to provide a significantly better fit of the experimental data. The parameters of the selected model for each peak were extracted as averages of the parameters of the repetitions.

4. Results

In eukaryotes, ubiquitinylation marks the proteins condemned to degradation, with ubiquitin being recognised and processed by the accessory proteins associated with the AAA+ unfoldase. In bacteria, a disordered protein N- or C-terminal tail of at least 10 amino acids is sufficient to guide proteins to proteolytic machinery. How substrates are recruited to the proteolytic machinery in archaea is still an open question. One hypothesis is that the small archaeal ubiquitin-like modifier protein (SAMP) has a similar role to ubiquitin in eukaryotes [34]. However, flexible and unstructured tails, of the kind used by bacteria, also function to target proteins to archaeal proteasomes *in vitro* [35] and may be relevant *in vivo* as well. In this work, to target the protein GFP to *Mj* PAN or PAN–20S proteasome complex, we added the bacterial ssrA tag (AANDENYALAA) to the C-terminus of GFP (GFP-ssrA) and used the resulting hybrid protein as a substrate of PAN.

*4.1.* **GFP-ssrA** *unfolding by PAN monitored by methyl-group NMR*

To follow the fate of the substrate protein during either the unfolding or the proteolytic reaction, we established an NMR-detected assay that monitored ∼100 methyl groups of GFP-ssrA during its processing by either *Mj* PAN or the *Mj* PAN–20S proteasome complex. In comparison to other methodologies used to measure unfolding kinetics, such as fluorescence spectroscopy [36,37], single-molecule force spectroscopy with optical tweezers [15,16,18], or contrast-matched time-resolved small-angle-neutron scattering (tr-SANS) [20,21], NMR offers the advantage of providing residue-specific information.

First, we prepared uniformly ^{15}N,[13]C-labelled GFP-ssrA (in the variant described in Materials and Methods) and assigned the ^{1}H and ^{13}C resonances for 119 out of the 133 GFP methyl-groups. Then, we prepared a sample containing 100 μM of ^{15}N,[13]C-labelled GFP-ssrA and 5 μM of unlabelled PAN in a buffer consisting of 20 mM Tris-HCl pH 7.5, 100 mM NaCl and 100 mM MgCl$_2$ in 90%:10% H$_2$O:D$_2$O. After initiating the unfolding reaction with the addition of 100 mM ATP and subsequent rapid transfer of the NMR

$$F_{avg} = \frac{\left((SS_{null,1} + SS_{null,2} + SS_{null,3}) - (SS_{alt,1} + SS_{alt,2} + SS_{alt,3})\right)/(SS_{alt,1} + SS_{alt,2} + SS_{alt,3})}{\left((DF_{null,1} + DF_{null,2} + DF_{null,3}) - (DF_{alt,1} + DF_{alt,2} + DF_{alt,3})\right)/(DF_{alt,1} + DF_{alt,2} + DF_{alt,3})} \tag{4}$$

where $SS_{null,1/2/3}$ are the fit-errors (sum-of-squares) of the model with a lower number of parameters (corresponding to the null-hypothesis, i.e. either ExpLin or ExpDec1) for the three repetitions 1, 2 and 3; $SS_{alt,1/2/3}$ are the fit-errors of the model with a higher

tube to the spectrometer probe (preheated at 60 °C), we recorded a series of 2D ^{1}H,[13]C-SOFAST-HMQC spectra [22]. The dead-time between the addition of ATP and the start of the data acquisition was 2.5–3 min. Each individual 2D spectrum was collected in ∼100 s (Fig. 1A). We used 100 mM ATP to ensure the presence of ATP throughout the entire time-course and 100 mM MgCl$_2$ as

high concentrations of magnesium were shown to boost the activity of AAA+ unfoldases [38,39]. These experiments can detect non-complexed GFP in solution and thus report on both the rate of unfolding and the presence of unfolding intermediates potentially released by PAN during the process.

We quantified the individual peak intensities I in each 2D $^1H,^{13}C$-SOFAST-HMQC spectrum and plotted them against the time t between the start of the acquisition of the first 2D spectrum and the start of the acquisition of each individual 2D spectrum. To obtain reliable time-constants for peak-specific intensity decays,
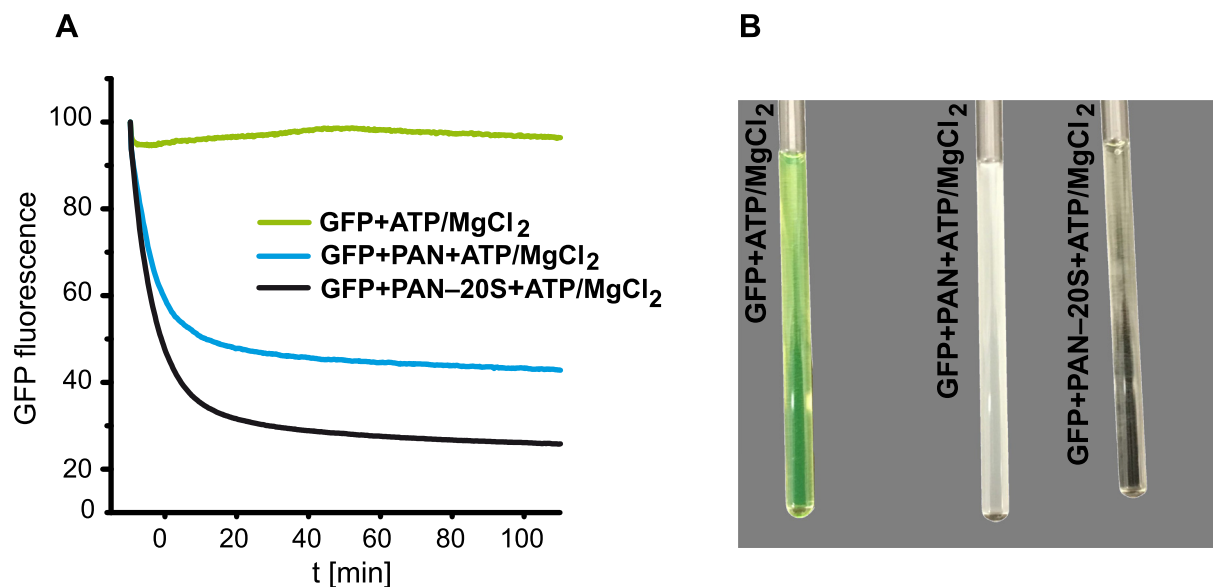
A

B
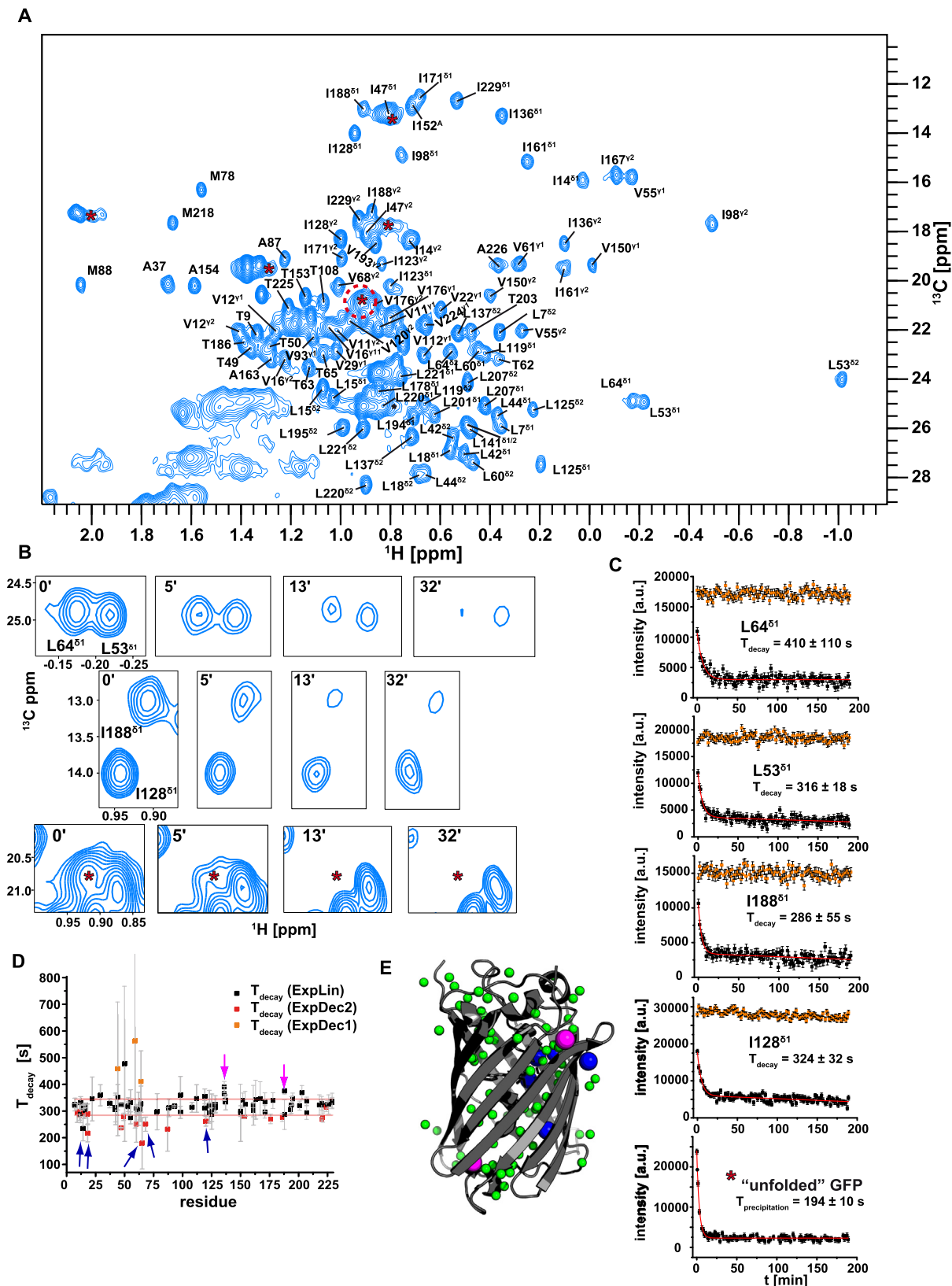
Fig. 2. Decay of GFP-ssrA fluorescence in the presence of either PAN or PAN–20S. A) Fluorescence decays of GFP-ssrA (100 μM) at 60 °C in the presence of 100 mM ATP and 100 mM MgCl$_2$ (green) and upon addition of either PAN (5 μM, light blue) or PAN–20S (5 μM, black). Fluorescence is a good indicator of GFP unfolding, as optical tweezers experiments have demonstrated that fluorescence is lost in the earliest events of the unfolding process [44]. The fluorescence values are scaled to 100 at the beginning of each reaction. The decays can be fitted by a biexponential function with shorter time-constants of 341 ± 12 s in the presence of PAN only ($T_{unfolding}$) and 243 ± 44 s in the presence of PAN–20S ($T_{proteolysis}$). The control experiment without PAN or PAN–20S does not show any appreciable decay and demonstrates that the GFP variant used in this study preserves its native fold for over 2 h at 60 °C. Fluorescence measurements were carried out in triplicate and the uncertainty corresponds to the standard error of the mean of the three fitted time-constants. B) NMR tubes containing the same reactants as in A) after incubation at 60 °C for 3 h. (For interpretation of the references to color in this figure legend, the reader is referred to the web version of this article.)

we fitted $I(t)$ to three different models and applied F-statistics to choose the function that reproduces the experimental data with the fewest parameters. The three models were: one exponential decay (ExpDec1, 3 parameters); two exponential decays (ExpDec2, 5 parameters); and one exponential plus one linear decay (ExpLin, 4 parameters). In total, we could analyse 102 methyl group peaks. For most peaks, $I(t)$ could not be fitted by one exponential decay but required the sum of either two exponential decays or an exponential and a linear decay (Fig. 1B and C). This behavior was observed before for the same unfolding reaction monitored by contrast-matched time-resolved SANS [20] and was attributed to the inhibitory effect of the increasing concentrations of ADP. Control experiments without PAN do not show any appreciable decay of the GFP peak intensities over time, testifying that the fold of the GFP variant used in this study is stable at 60 °C for the entire duration of the experiment. For 90% of all evaluated peaks, the shortest time constant T_{decay} was within the range of one standard deviation (SD) from the mean (Fig. 1C). The value of the mean T_{decay} = 314 ± 30 s is in good agreement with that obtained from fluorescence-detected (Fig. 2) or SANS-detected experiments conducted under similar conditions [20]. Besides I47-δ1 and L220-δ1, which overlap with new peaks appearing in the random-coil region of the spectrum (*vide infra*), another seven peaks decayed

either faster (I14-δ1, L18-δ2, T65-γ2, V68-γ2, V120-γ2) or slower (I136-δ1 and I188-γ2) than average. Because these methyl groups are scattered over the entire GFP structure (Fig. 1D), their slightly different decay time-constants cannot be indicative of the presence in solution of sequentially, partially-unfolded intermediates released by PAN and must be the result of experimental uncertainties. Thus, we conclude that GFP is either cooperatively unfolded by PAN or that any partially unfolded intermediates are either not released from the PAN or, if released, refold rapidly to the native conformation.
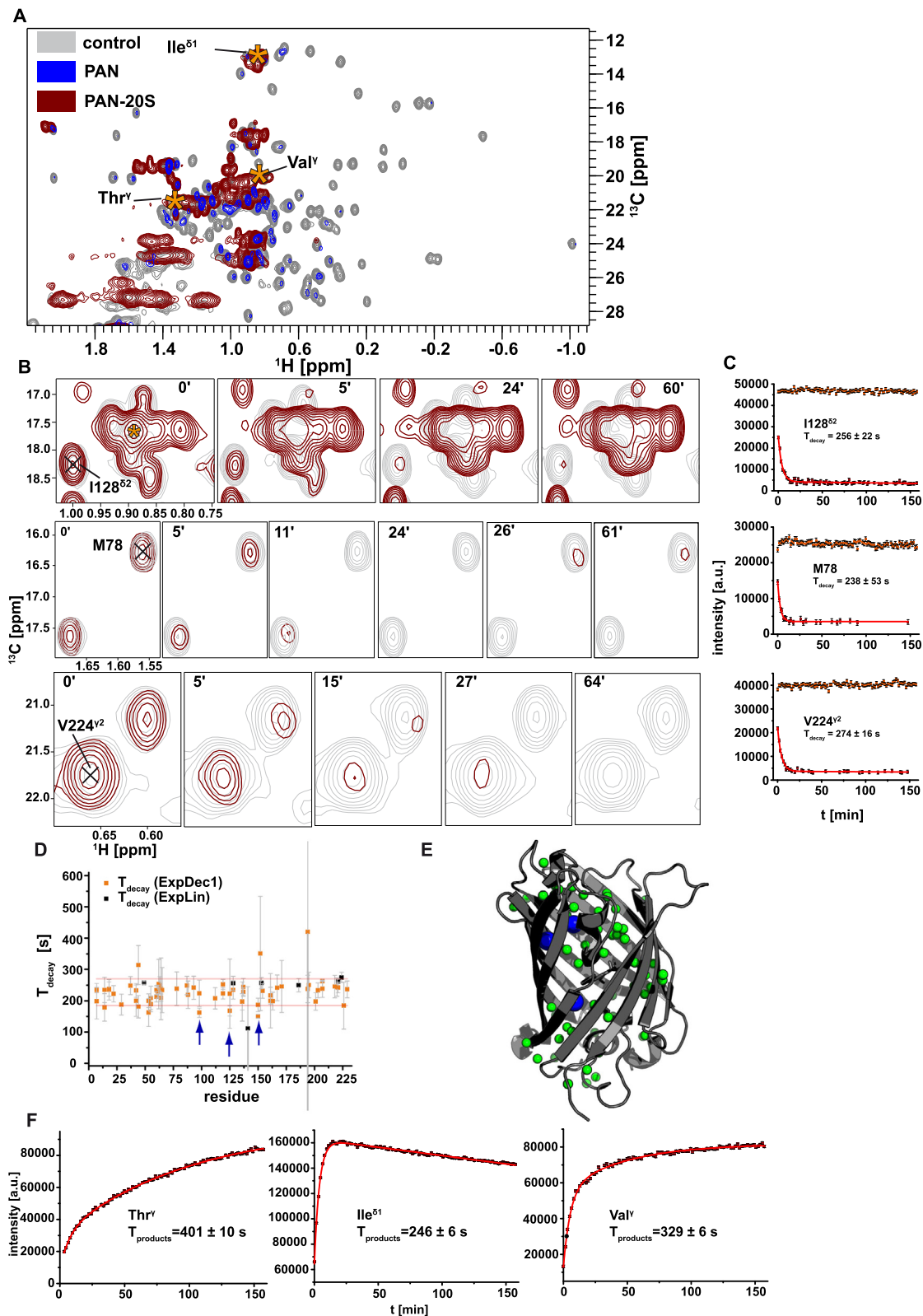
In the first few spectra of the time-course, we observed new peaks at positions corresponding to the random-coil shifts of Ala, Ile, Leu, Met and Val methyl groups (Fig. 1A), which then disappeared at later time-points. These peaks belong to unfolded GFP released by PAN after translocation, which then aggregates and precipitates out of solution as its concentration increases. The appearance of a white precipitate in the NMR tubes containing GFP-ssrA, PAN, ATP and MgCl$_2$ after incubation at 60 °C confirmed this interpretation (Fig. 2B). The time-dependent intensity profile of the one random-coil peak that was not overlapped with native GFP peaks (δ(^{1}H) = 0.92 ppm; δ(^{13}C) = 20.8 ppm, Fig. 1A) could be fit to a single exponential with a time-constant $T_{precipitation}$ of 179 ± 10 s. Thus, we conclude that the unfolding process of GFP

◄

Fig. 1. Processing of GFP-ssrA by PAN. A) SOFAST-^{13}C-HMQC spectrum of the GFP-ssrA methyl region with peak assignments. As we have no stereospecific assignment for the LV methyl groups, the labels δ1/δ2 and γ1/γ2 are used only to distinguish the two methyl groups of each residue. The spectrum shown is the first of a time-course to monitor the unfolding of GFP-ssrA (100 μM) by PAN (5 μM) in the presence of ATP and MgCl$_2$ (100 mM each) at 60 °C. Asterisks indicate peaks appearing in the random-coil regions of ILVM methyl groups. B) Selected regions of ^{1}H,^{13}C-SOFAST-HMQC spectra at different time-points (in minutes) during the unfolding reaction. The red asterisk indicates a peak attributed to unfolded GFP-ssrA. C) Decay curves of the peaks in B) showing peak intensities extracted from control runs (orange, w/o PAN) and unfolding runs (black). Errors were estimated from the spectral noise. The fitted curve is shown in red; the shortest exponential time-constant T_{decay} is given as a mean of triplicate measurements with uncertainty corresponding to the standard error of the mean. a.u., arbitrary units. D) Shortest exponential time-constants T_{decay} for all analysed peaks. Each peak is represented by a square, which is color-coded according to the function used to fit its decay. The average T_{decay} of all peaks is 314 ± 30 s (range indicated by the pink lines). The peaks with T_{decay} values smaller or larger than the average T_{decay} by more than one standard deviation are indicated by blue and pink arrows, respectively. E) Representation of ranges of T_{decay} values for all analysed methyl groups on the GFP-crystal structure (PDB entry 2B3Q). Methyl groups with T_{decay} values close to, smaller or larger than the average are indicated in green, blue and pink, respectively. (For interpretation of the references to color in this figure legend, the reader is referred to the web version of this article.)

by PAN, in the absence of the 20S proteasome, generates unfolded and aggregation-prone GFP molecules, which, after reaching a critical concentration, fall out of solution almost twice as fast ($T_{precipitation}$ = 179 ± 10 s) as the native GFP is unfolded (T_{decay} = 314 ± 30 s).

4.2. GFP-ssrA degradation by the PAN–20S proteasome complex

We then measured time-resolved 2D SOFAST-^{13}C-HMQC spectra of a sample containing 100 μM ^{15}N,^{13}C-labelled GFP-ssrA and 5 μM PAN–20S proteasome complex (Fig. 3A). The buffer composi-

tion and the experimental set-up were the same as described above. In the presence of the 20S proteasome, the intensity decay of the native GFP peaks was faster with a mean time constant T_{decay} of 227 ± 42 s (Fig. 3B, C), in agreement with earlier reports demonstrating that the coupling to the CP stimulates the activity of the unfoldase [40]. Consequently, we could analyse only 69 peaks in a quantitative manner. Most decay curves could be fit with a single-exponential model, probably due to the very low signal-to-noise at the later time-points, which masked the presence of a second exponential decay with higher time constant. Nearly all peaks decayed with a time constant within the mean ± 1 SD, except for I98-γ2, L125-δ1 and V150-γ2, which decayed slightly faster (Fig. 3C, D).

In the presence of the 20S CP, the intensities of the peaks appearing in the random-coil region grew with time until they reached a plateau (Fig. 3A, F). We attribute these peaks to short, unfolded peptides, which originate from protein digestion by PAN–20S. These short protein fragments do not aggregate and do not precipitate out of solution. In agreement, at the end of the reaction, the NMR tube contained a clear solution, from which the fluorescence of the GFP had been lost but in which no precipitate was formed (Fig. 2B). We could fit the time-dependence of the intensities of 23 such peaks and obtained an average $T_{products}$ of 355 ± 155 s (Fig. 3F). The fact that this time-constant is of the same order-of-magnitude as the time-constant of the decay of GFP peaks (T_{decay} = 227 ± 42 s), suggests a tight coupling of the unfolding and degradation processes in the proteolysis reaction.

Finally, datasets recorded at 55 °C gave similar results, albeit with slower decay times (average T_{decay} with PAN alone, 426 ± 67 s; average T_{decay} with PAN–20S CP, 419 ± 78 s) (Fig. 4). Interestingly, at this lower temperature, the 20S CP had lost its capacity to stimulate PAN activity, as the time-constants measured with and without the 20S CP were virtually identical.

5. Discussion

Our time-resolved NMR data demonstrate that in the absence of the 20S CP, the PAN unfoldase processes GFP without releasing any long-lived unfolding intermediates into solution. Optical tweezers experiments have shown that bacterial ClpX unfolds GFP in three steps, passing through two short-lived intermediates (<240 ms), where β-strands 7–11 are unfolded first [15,18]. On the other hand, cooperative unfolding of globular domains has been reported for GB1 and for the N-terminal domain of calmodulin unfolded by the archaeal AAA+ ATPase VAT [19]. Our experiments cannot discriminate whether PAN unfolds GFP cooperatively or by passing through short-lived intermediates, as our experimental approach is unable to reveal short-lived GFP intermediates bound to PAN. However, we can confidently exclude the presence of unbound, long-lived (i.e. with a life-time much longer than the difference in the chemical shifts of the folded and unfolded species) unfolding

intermediates in concentrations equal or above our detection limits (estimated to be ∼ 10 μM). This is indicated both by the similar time constants of decay of all GFP peaks and by the absence of any peaks at frequencies close to but distinct from those of the native GFP peaks. This result is consistent with that of SANS experiments, showing that the fraction of partially unfolded GFP is always <5–10% of the total substrate. However, it should be noted that the SANS data report on the presence of both PAN-bound and unbound unfolding intermediates, while the NMR experiments detect only unbound species. Combining the NMR and SANS results, it is reasonable to conclude that the concentration of long-lived unfolding intermediates released by PAN before completing the translocation process is vanishingly small. This is important in a cellular context, where the release of partially denatured substrates could lead to the formation of aggregates toxic to the cell and should thus be avoided.

In contrast to literature data, which shows that at 30 °C denatured GFP released from stalled ClpXP refolds at a rate comparable to that of denaturation [41], we do not see any evidence of refolding of GFP to its native state after translocation through PAN. In contrast, after reaching a critical concentration, unfolded GFP aggregates and precipitates out of solution at a rate twice as fast as the unfolding rate. This discrepancy may be due to the high temperature of our assay (60 °C) at which GFP refolding may be slower than at 30 °C.

In the presence of the 20S proteasome, native GFP peaks decay with a time-constant T_{decay} of 227 ± 27 s, faster than in the presence of PAN alone (T_{decay} = 314 ± 30 s), demonstrating that degradation occurs faster than unfolding and translocation. If degradation were slower than translocation, PAN would not be able to release the unfolded substrate molecule into the proteasome chamber until the proteasome has finished processing the previous molecule, which would lead to a slower, rather than faster, decay of native GFP. The faster native GFP decay rate suggests that the presence of the 20S CP stimulates substrate turn-over by PAN. Because the 20S CP has been shown to associate with PAN only transiently [42], our data favor the hypothesis that substrate binding assists the docking of the 20S CP with PAN and that this, in turn, stimulates PAN activity.

Previous studies have demonstrated that bacterial AAA + ATPases engage the substrate in several futile unfolding attempts, after which the destabilized substrate is released into solution [43]. The number of unsuccessful attempts depends on substrate stability. Our experiments show that if destabilized GFP is released into solution after unsuccessful unfolding attempts, it either rapidly returns to the native state, even at 60 °C, or is present at very low concentrations (<10%).

Notably a temperature reduction of only 5 °C leads to ∼25% slower decay rates and to loss of 20S CP-dependent stimulation of PAN activity. This finding suggests that PAN activity depends on dynamic processes that become less efficient at lower temperature and also loosen their coupling to proteasome docking. An

---

Fig. 3. PAN–20S degrades GFP-ssrA into small soluble peptides. A) Overlay of the last time-resolved SOFAST-^{13}C-HMQC spectra of GFP-ssrA at the end of a control reaction (100 μM GFP-ssrA, 100 mM MgCl$_2$, 100 mM ATP, grey), an unfolding reaction (100 μM GFP-ssrA, 5 μM PAN, 100 mM MgCl$_2$, 100 mM ATP, blue) and a proteolysis reaction (100 μM GFP-ssrA, 5 μM PAN–20S, 100 mM MgCl$_2$, 100 mM ATP, dark red). The asterisks mark the peaks corresponding to Ile, Val and Thr random-coil methyl groups. B) Selected regions of SOFAST-^{13}C-HMQC spectra (dark red) at different time-points (in minutes) during the proteolysis reaction, overlaid with spectra of the control reaction (without PAN–20S, grey). The asterisk marks a peak corresponding to a random-coil methyl group. C) Decay curves of peaks in B) from the control reaction (orange, without PAN–20S) and from the proteolysis reaction (black). Errors were estimated from the spectral noise. The fitted curve is in red; the exponential time-constant T_{decay} is given as a mean of triplicate measurements with uncertainty corresponding to the standard error of the mean. D) Exponential time-constants T_{decay} for all analysed peaks. Each peak is represented by a square, which is color-coded according to the function used to fit its decay. The average T_{decay} of all peaks is 227 ± 42 s (range indicated by the pink lines). Blue arrows indicate peaks whose T_{decay} values are smaller than the average by more than one SD. E) Representation of ranges of T_{decay} values for all analysed methyl groups on the GFP-crystal structure (PDB entry 2B3Q). Methyl groups with T_{decay} values close to or smaller than the average are shown in green and blue, respectively. F) Growth curves of peaks attributed to unstructured proteolysis products with their exponential fits and shortest time-constants $T_{products}$. (For interpretation of the references to color in this figure legend, the reader is referred to the web version of this article.)
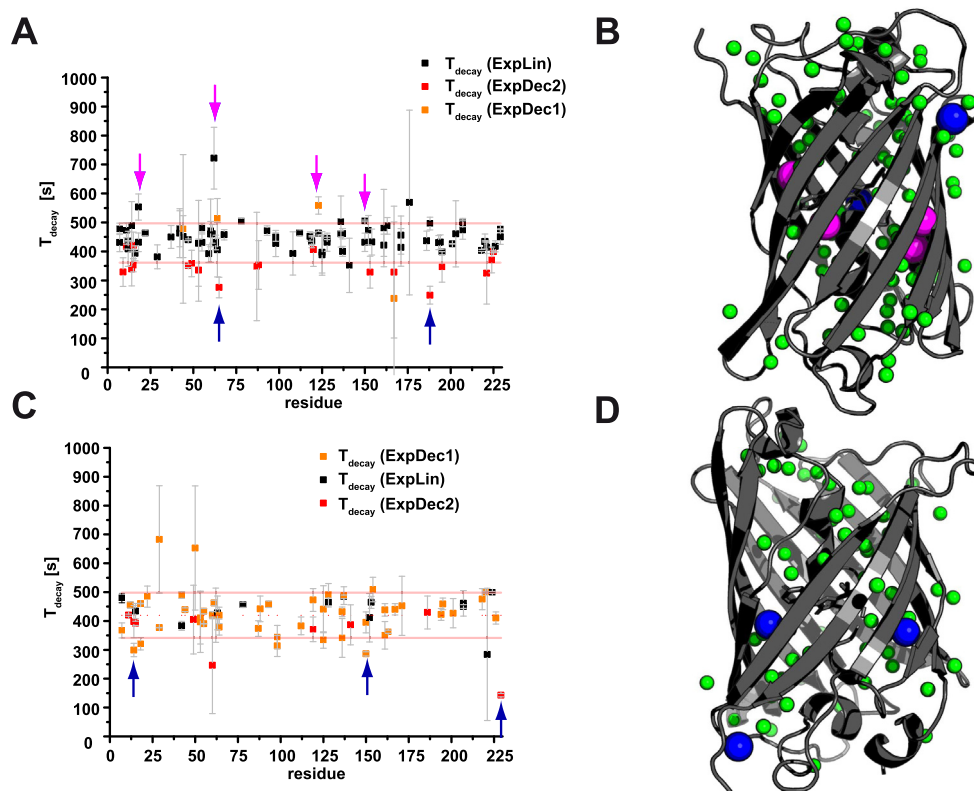
Fig. 4. Unfolding and proteolysis time-constants at 55 °C. A) Shortest exponential time-constants, T_{decay}, for all methyl-group peaks analysed over time-resolved SOFAST-^{13}C-HMQC spectra of GFP-ssrA (100 μM) in the presence of PAN (5 μM), ATP (100 mM) and MgCl$_2$ (100 mM) at 55 °C. Each methyl-group peak is represented by a square, which is color-coded according to the function used to fit its decay. The average T_{decay} of all peaks is 426 ± 67 s; this range is indicated by the pink lines. The peaks whose T_{decay} are smaller or larger than the average T_{decay} by more than one standard deviation are indicated by blue and pink arrows, respectively. B) Representation of ranges of T_{decay} values of A) on the GFP crystal structure (PDB entry 2B3Q). Methyl groups with T_{decay} time-constants close to, smaller or larger than the average are indicated in green, blue and pink, respectively. C) Shorter exponential time-constants, T_{decay}, for all methyl-group peaks analysed over time-resolved SOFAST-^{13}C-HMQC spectra of GFP-ssrA (100 μM) in the presence of PAN–20S (5 μM), ATP (100 mM) and MgCl$_2$ (100 mM) at 55 °C. Each methyl-group peak is represented by a square, which is color-coded according to the function used to fit its decay. The average T_{decay} of all peaks is 419 ± 78 s; this range is indicated by the pink lines. The peaks whose T_{decay} are smaller than the average T_{decay} by more than one standard deviation are indicated by blue arrows. D) Representation of ranges of T_{decay} values of C) on the GFP crystal structure (PDB entry 2B3Q). Methyl groups with T_{decay} time-constants close to or smaller than the average are indicated in green and blue, respectively. (For interpretation of the references to color in this figure legend, the reader is referred to the web version of this article.)

area of future research will focus on the identification and characterization of these dynamics and on understanding how these processes are optimized to work at high temperature in thermophilic organisms.

6. Conclusions

We have exploited an NMR-detected assay to monitor PAN-dependent unfolding of GFP with atomic resolution. The timescale of the NMR experiments provides a resolution of ∼100 s. We demonstrate that the process of GFP unfolding does not involve release of measurable quantities of long-lived unfolding intermediates in solution, either in the presence or in the absence of the 20S proteasome. We find that the presence of the 20S CP stimulates PAN activity at 60 °C, while this regulation is lost at moderately lower temperatures. We show that, even if previous literature has demonstrated that archaeal PAN and 20S CP do not form a stable complex, the presence of the substrate tethers the 20S CP to the PAN for a time long enough to tightly couple the unfolding and degradation processes, thus avoiding the formation of toxic aggregates that would result from release of denatured protein after translocation.

Data availability

Data will be made available on request.

Declaration of Competing Interest

The authors declare that they have no known competing financial interests or personal relationships that could have appeared to influence the work reported in this paper.

Acknowledgements

References

[1] A.L. Goldberg, Protein degradation and protection against misfolded or damaged proteins, Nature 426 (6968) (2003) 895–899.

[2] R.S. Yedidi, P. Wendler, C. Enenkel, AAA-ATPases in Protein Degradation, Front. Mol. Biosci. 4 (42) (2017).

[3] B. Chen et al., Cellular Strategies of Protein Quality Control, Cold Spring Harb. Perspect. Biol. 3 (8) (2011).

[4] P. Majumder, W. Baumeister, Proteasomes: unfoldase-assisted protein degradation machines, Biol. Chem. 401 (1) (2019) 183–199.

[5] C.M. Pickart, R.E. Cohen, Proteasomes and their kin: proteases in the machine age, Nat. Rev. Mol. Cell Biol. 5 (3) (2004) 177–187.

[6] D.H. Wolf, R. Menssen, Mechanisms of cell regulation - proteolysis, the big surprise, FEBS Lett. 592 (15) (2018) 2515–2524.

[7] A.H. de la Peña et al., Substrate-engaged 26S proteasome structures reveal mechanisms for ATP-hydrolysis–driven translocation, Science 362 (6418) (2018) eaav0725.

[8] Y. Dong et al., Cryo-EM structures and dynamics of substrate-engaged human 26S proteasome, Nature 565 (7737) (2019) 49–55.

[9] G.C. Lander et al., Complete subunit architecture of the proteasome regulatory particle, Nature 482 (7384) (2012) 186–191.

[10] M.E. Matyskiela, G.C. Lander, A. Martin, Conformational switching of the 26S proteasome enables substrate degradation, Nat. Struct. Mol. Biol. 20 (7) (2013) 781–788.

[11] P.Sledz et al., Structure of the 26S proteasome with ATP-gamma S bound provides insights into the mechanism of nucleotide-dependent substrate translocation. In: Proceedings of the National Academy of Sciences of the United States of America, 2013 110(18) 7264-7269.

[12] X. Huang et al., An atomic structure of the human 26S proteasome, Nat. Struct. Mol. Biol. 23 (9) (2016) 778–785.

[13] P. Unverdorben et al., Deep classification of a large cryo-EM dataset defines the conformational landscape of the 26S proteasome, Proc. Natl. Acad. Sci. U.S.A. 111 (15) (2014) 5544–5549.

[14] P. Majumder et al., Cryo-EM structures of the archaeal PAN-proteasome reveal an around-the-ring ATPase cycle, Proc. Natl. Acad. Sci. U.S.A. 116 (2) (2019) 534–539.

[15] R.A. Maillard et al., ClpX(P) generates mechanical force to unfold and translocate its protein substrates, Cell 145 (3) (2011) 459–469.

[16] M.E. Aubin-Tam et al., Single-molecule protein unfolding and translocation by an ATP-fueled proteolytic machine, Cell 145 (2) (2011) 257–267.

[17] J.C. Cordova et al., Stochastic but highly coordinated protein unfolding and translocation by the ClpXP proteolytic machine, Cell 158 (3) (2014) 647–658.

[18] M. Sen et al., The ClpXP protease unfolds substrates using a constant rate of pulling but different gears, Cell 155 (3) (2013) 636–646.

[19] R. Augustyniak, L.E. Kay, Cotranslocational processing of the protein substrate calmodulin by an AAA+ unfoldase occurs via unfolding and refolding intermediates, Proc. Natl. Acad. Sci. U.S.A. 115 (21) (2018) E4786–E4795.

[20] E. Mahieu et al., Observing Protein Degradation by the PAN-20S Proteasome by Time-Resolved Neutron Scattering, Biophys. J. 119 (2) (2020) 375–388.

[21] Z. Ibrahim et al., Time-resolved neutron scattering provides new insight into protein substrate processing by a AAA+ unfoldase, Sci. Rep. 7 (2017) 40948.

[22] P. Schanda, Ē. Kupče, B. Brutscher, SOFAST-HMQC Experiments for Recording Two-dimensional Heteronuclear Correlation Spectra of Proteins within a Few Seconds, J. Biomol. NMR 33 (4) (2005) 199–211.

[23] F. van den Ent, J. Löwe, RF cloning: A restriction-free method for inserting target genes into plasmids, J. Biochem. Bioph. Methods 67 (1) (2006) 67–74.

[24] G.S. Waldo et al., Rapid protein-folding assay using green fluorescent protein, Nat. Biotechnol. 17 (7) (1999) 691–695.

[25] D.A. Zacharias et al., Partitioning of Lipid-Modified Monomeric GFPs into Membrane Microdomains of Live Cells, Science 296 (5569) (2002) 913–916.

[26] A. Velyvis, A.M. Ruschak, L.E. Kay, An economical method for production of (2) H, (13)CH3-threonine for solution NMR studies of large protein complexes: application to the 670 kDa proteasome, PLoS One 7 (9) (2012) e43725.

[27] F. Delaglio et al., NMRPipe: A multidimensional spectral processing system based on UNIX pipes, J. Biomol. NMR 6 (3) (1995) 277–293.

[28] W.F. Vranken et al., The CCPN data model for NMR spectroscopy: Development of a software pipeline, Proteins Struct. Funct. Bioinf. 59 (4) (2005) 687–696.

[29] J. Santoro et al., Constant-time NOESY: An aid in the analysis of protein NMR spectra, J. Biomol. NMR 2 (6) (1992) 647–653.

[30] G.W. Vuister, A. Bax, Resolution enhancement and spectral editing of uniformly 13C-enriched proteins by homonuclear broadband 13C decoupling, J. Magn. Reson. 98 (1992) 428–435.

[31] A. Bax, G.M. Clore, A.M. Gronenborn, 1H-1H correlation via isotropic mixing of 13C magnetization, a new three-dimensional approach for assigning 1H and 13C spectra of 13C-enriched proteins, J. Magnetic Resonance (1969) 88 (2) (1990) 425–431.

[32] G.T. Montelione et al., An efficient triple resonance experiment using carbon-13 isotropic mixing for determining sequence-specific resonance assignments of isotopically-enriched proteins, J. Am. Chem. Soc. 114 (27) (1992) 10974–10975.

[33] C. Amero et al., Fast Two-Dimensional NMR Spectroscopy of High Molecular Weight Protein Assemblies, J. Am. Chem. Soc. 131 (10) (2009) 3448–3449.

[34] J. Maupin-Furlow, Proteasomes and protein conjugation across domains of life, Nat. Rev. Microbiol. 10 (2) (2012) 100–111.

[35] D. Berko et al., The Direction of Protein Entry into the Proteasome Determines the Variety of Products and Depends on the Force Needed to Unfold Its Two Termini, Mol. Cell 48 (4) (2012) 601–611.

[36] N. Benaroudj, A.L. Goldberg, PAN, the proteasome-activating nucleotidase from archaebacteria, is a protein-unfolding molecular chaperone, Nat. Cell Biol. 2 (11) (2000) 833–839.

[37] A. Snoberger, R.T. Anderson, D.M. Smith, The Proteasomal ATPases Use a Slow but Highly Processive Strategy to Unfold Proteins, Front. Mol. Biosci. 4 (2017) 18.

[38] A. Gerega et al., VAT, the thermoplasma homolog of mammalian p97/VCP, is an N domain-regulated protein unfoldase, J. Biol. Chem. 280 (52) (2005) 42856–42862.

[39] R. Golbik et al., The Janus Face of the Archaeal Cdc48/p97 Homologue VAT: Protein Folding versus Unfolding. 1999. **380**(9): p. 1049-1062.

[40] F. Zhang et al., Mechanism of substrate unfolding and translocation by the regulatory particle of the proteasome from Methanocaldococcus jannaschii, Mol. Cell 34 (4) (2009) 485–496.

[41] Y.-I. Kim et al., Dynamics of Substrate Denaturation and Translocation by the ClpXP Degradation Machine, Mol. Cell 5 (4) (2000) 639–648.

[42] D.M. Smith et al., ATP Binding to PAN or the 26S ATPases Causes Association with the 20S Proteasome, Gate Opening, and Translocation of Unfolded Proteins, Mol. Cell 20 (5) (2005) 687–698.

[43] A.O. Olivares, T.A. Baker, R.T. Sauer, Mechanistic insights into bacterial AAA+ proteases and protein-remodelling machines, Nat. Rev. Microbiol. 14 (1) (2016) 33–44.

[44] Z. Ganim, M. Rief, Mechanically switching single-molecule fluorescence of GFP by unfolding and refolding, PNAS 114 (42) (2017) 11052–11056.